

*Experimental Verification of the Three-dimensional Thermal-Hydraulic Models in the Best-Estimate Code BAGIRA

S.D.Kalinichenko¹, A.E.Kroshilin¹, V.E.Kroshilin¹, A.V.Smirnov¹, and P.Kohut²

¹All-Russian Research Institute for Nuclear Power Plants (VNIIAES),
25 Ferganskaya St., 109507 Moscow, Russia

²Brookhaven National Laboratory, Bldg. 475 Upton, NY 11973
Tel: 631-344-4982, Fax: 631-344-1430, Email: kohut@bnl.gov

Abstract – *In this paper we present verification results of the BAGIRA code that was performed using data from integral thermal-hydraulic experimental test facilities as well as data obtained from operating nuclear power plants. BAGIRA is a three-dimensional numerical best-estimate code that includes non-homogeneous modeling. Special consideration was given to the recently completed experimental data from the PSB-VVER integral test facility (EREC, Electrogorsk, Russia) – a new Russian large-scale four-loop unit, which has been designed to model the primary circuits of VVER-1000 type reactors. It is demonstrated that the code BAGIRA can be used to analyze nuclear reactor behavior under normal and accident conditions.*

I. INTRODUCTION

One of the most important and notoriously difficult problems in developing a modern thermal-hydraulic best-estimate code is the consistent incorporation of multi-dimensional flow models. The results of many numerical studies indicated that using one-dimensional approach in modeling wide range of physical processes affecting nuclear power plant (NPP) operation is insufficient. Multi-dimensional effects must be considered in modeling flow regimes with the following characteristics:

- Asymmetrical changes in coolant mass flow-rate in one or several loops;
- Removal of one or more primary loops from plant operation;
- Loss of heat removal from the secondary circuit;
- Insertion of positive or negative reactivity in a limited region of the reactor core;
- Containment spray systems malfunction.

During the last decade, VNIIAES has developed BAGIRA, a three-dimensional numerical best-estimate thermal-hydraulic code that includes non-homogeneous models. BAGIRA is used for modeling various physical processes in operating nuclear reactors under normal, abnormal, transients and accident operations, including

severe accident events. An effective numerical algorithm allows the code to perform real-time calculations, using multi-dimensional nodalization for the reactor vessel and steam generators (SG's), which is useful in operator training.

In the initial development stage, BAGIRA was carefully verified using data available from laboratory experiments, integral test facilities, and to a limited extent using data from operating nuclear power plants.

Reference 1 includes more detailed information about the basic assumptions in the physical models, the system of initial equations, the principles of numerical scheme, and preliminary results of validation tests.

In Section II-IV, we will present the verification of the multidimensional two-phase flow models for real NPP's. In Section V we describe the results of numerical analysis performed using data obtained from recent one-dimensional experiments performed at the large-scale integral test facility PSB-VVER. This is the most up-to-date Russian test experiment intended for modeling the primary circuit of a typical VVER-1000 type reactor.

II. REACTOR COOLANT PUMP SHUTDOWN TESTS

An important case where significant multidimensional effects play an important role is shutting down one or two main reactor coolant pumps

(RCP) in the primary circuit of a VVER-1000 reactor vessel.

After a RCP is shut off (will be referred as the “stagnant” loop) the coolant flow will reverse in the loop and water will enter to the reactor vessel from the “hot” leg. Since the four loops are joined to different parts of the vessel, the coolant temperature inside the upper plenum of the vessel near the junction point of the “stagnant” loop becomes lower than in the other regions. Due to turbulent mixing the low temperature zone spreads gradually to the regions where two other loops closest to the “stagnant” loop join the reactor vessel. The coolant temperature in the fourth loop, which is the farthest from the “stagnant” loop, will practically remain the same until the low temperature zone reaches the fourth loop junction region. Thus, the non-uniformity of the coolant temperature distribution in the horizontal cross section of the upper plenum of the reactor vessel leads to an asymmetry in the behavior of the three loops with the normally operating RCP’s. Note that even after a quasi-stationary flow regime is established, the non-uniformity in the temperature distribution, mentioned above, will not disappear. The non-uniform temperature effect has been observed by NPP operators.

In order to model the asymmetric temperature distribution inside the reactor vessel, we used a plant specific analytical simulator, which uses the three-dimensional (3-D) BAGIRA code for calculating the thermal-hydraulic behavior of the primary circuit. Figure 1 indicates the 3-D rectangular nodalization scheme as was applied to the reactor vessel. It contains 7×7 cells in the horizontal x - y plane and 7 cells along the z axis. The cell sizes are indicated in meters. The cells shown by gray color belong to the inner part of the vessel, i.e. coolant flows through them, while the cells shown by white color lie beyond the vessel and can be neglected in the analysis. This scheme allows approximating the vessel geometry by means of a set of rectangular cells. Figure 2 indicates the calculated reactor coolant temperature distribution above the reactor core after two RCP’s were successively shut down. As expected, the distribution has a distinct maximum that is shifted to the adjoining vessel region with the operating RCP’s.

It is important to note that a one-dimensional approach would not allow the modeling of the non-uniform coolant temperature distribution in the horizontal cross section of the reactor vessel while BAGIRA with its 3-D numerical capabilities can model and describe non-uniform asymmetric phenomenon.

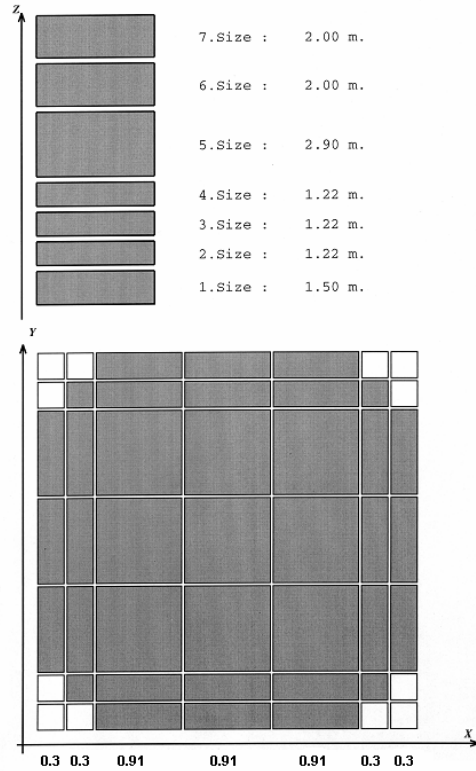


Fig. 1 VVER-1000 reactor vessel nodalization scheme

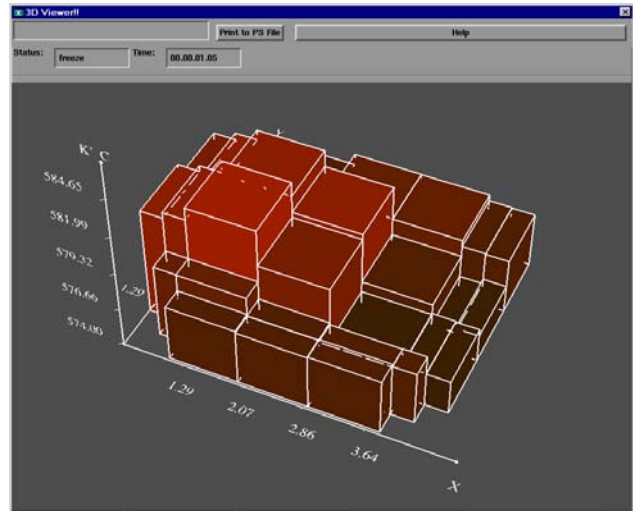


Fig. 2 Coolant temperature distribution above the reactor core, two RCPs shutdown
III. STEAM GENERATOR

III.A. Description

The second example in demonstrating the importance of multidimensional effects of reactor coolant

flow is the experiment performed at the Unit No. 5 of Novovoronezh NPP², where coolant parameters in the horizontal steam generator (SG) were measured. In the experiment, the dependency of the volumetric water-vapor mixture velocity and void fraction on the reactor power were measured. The physical location of measurements was in the gap between the SG vessel and the “hot” side of the heat-exchange tube bundle.

The SG cross section is shown schematically in Fig. 3. The primary circuit coolant enters the cylindrical inlet header, then goes through the horizontal heat exchange tube bundle and collects in the outlet header. Steam demand is balanced with the help of a perforated plate installed above the heat exchange tubes. Two vertical submerged shields are also placed between the SG vessel and the “hot” and “cold” parts of the tube bundle. Feed water comes through 16 inlet pipes entering the SG vessel between the perforated plate and heat exchange tubes. Steam moves through the separator and enters the steam collector. The design is based on the assumption that during normal operation the coolant moves down in the gap between the vessel and the submerged shield on the “hot” side of the bundle.

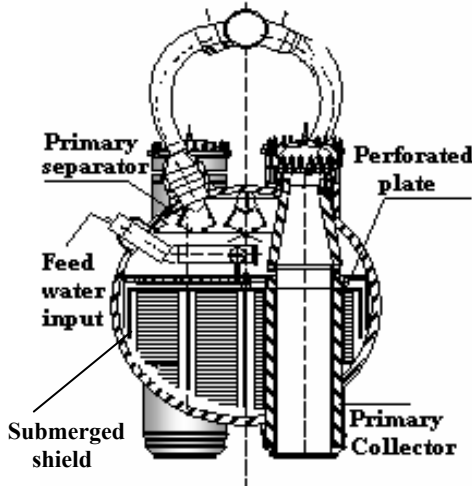


Fig. 3 SG cross section

The measurements revealed quite different coolant flow pattern in the secondary circuit near the inlet header. In the gap, between the SG vessel and the submerged shield on the “hot” side, a steady rising flow occurs. Under such conditions water flows from the gap into the space above the perforated plate that increases steam humidity and reduces its quality. This flow pattern can not be correctly described by one-dimensional calculations requiring a multi-dimensional approach.

III.B. Numerical scheme

The SG length reasonably exceeds its width, and the longitudinal gradients of coolant parameters are much

smaller than the transversal ones. For this reason the characteristic transversal flux velocities are greater than the longitudinal ones at least by an order of magnitude. Taking this into account, we used a model with a two-dimensional nodalization scheme, which allows the modeling of coolant flow in the SG cross section by neglecting the longitudinal flux. Specifically we considered the cross section near the inlet (“hot”) header because at this cross section there is a strong difference in the specific thermal flux at the heat-exchanger tube-bundle (the thermal fluxes from the “hot”, “middle” and “cold” parts are in the ratio of 4:2.5:1).

The SG nodalization scheme is shown in Fig. 4. It includes all important SG elements: the “hot” (between the first and the second layers in X-direction) and “cold” (between the last and next-to-last layers in X-direction), submerged shields, the perforated plate (between the 5-th and 6-th layers in Z-direction), the “hot” ($X = 2$), “middle” ($X = 4$), “cold” ($X = 6$) parts of the tube-bundle, and the channels between the heat-exchanger tubes ($X = 3, X = 5$). Feed water is injected at layer $Z = 5$, and due to the special method of feed water injection, the specific feed water flow-rates in the 2nd and 3rd layers ($X = 2, 3$) are equal to each other, while the flow-rate in the 4-th layer ($X = 4$) is half of the other two layers.

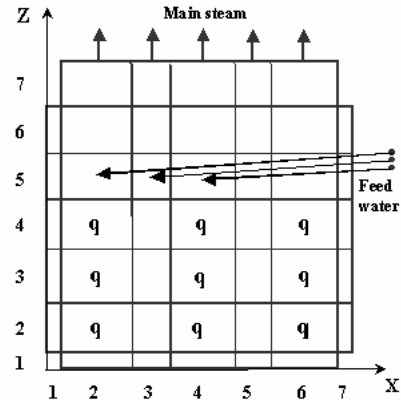


Fig. 4 SG nodalization scheme

III.C. Comparison with experimental data

In Fig. 5 the calculated water velocity profile is shown for rated SG operating conditions. The analysis predicts a global water circulation pattern in the whole SG cross section. In the “cold” sections, the coolant moves downward, while in the “hot” and middle sections the flow rises due the reduced density of hot water. In the gap, between the SG vessel and the submerged shield, the coolant is rising which contradicts the SG design assumptions for the operating regime. The main reason for this phenomenon is due to vapor generation in the gap region

near the “hot” tube bundle as the vapor in all layers moves upwards.

In Fig. 6 the calculated mixture volumetric velocity profile is shown again for rated SG operating conditions. In general, the mixture volumetric velocity profile is analogous to the water velocity distribution (see Fig. 5) with some specific differences. The vertical component of the water velocity near the perforated plate (both above and below) is close to zero, while the vertical component of the mixture volumetric velocity, in the same region, is quite significant at 0.5 m/s. We have also calculated the coolant flow parameters for lower reactor power values, which indicated that the main qualitative features of the flow pattern remain similar to the pattern seen at the nominal power value.

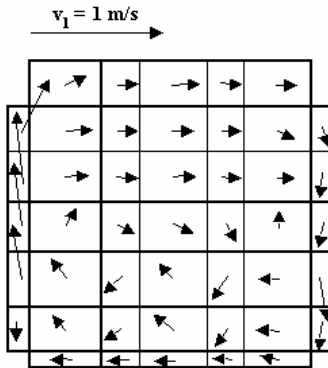


Fig. 5 Water velocity profile (analysis)

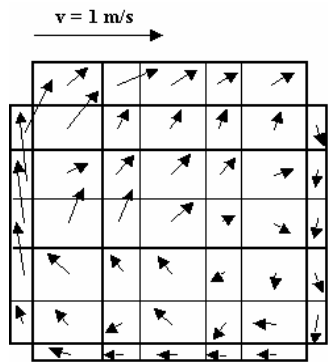


Fig. 6 Volumetric mixture velocity profile (analysis)

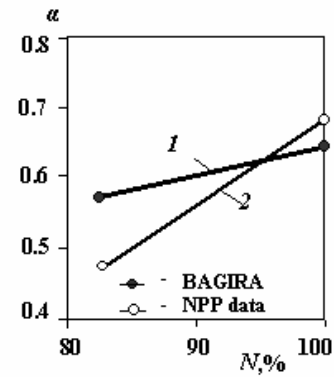


Fig. 7 Dependence of volumetric velocity on power, in the gap between the SG vessel and the “hot” submerged shield

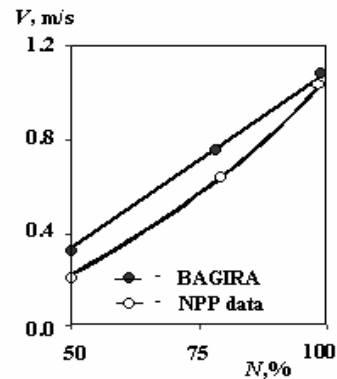


Fig. 8 Void fraction vs. power, in the gap between the SG vessel and the “hot” submerged shield

Figures 7 and 8 show a comparison of the calculated and experimental parameter dependencies on the relative reactor power in the gap between the SG vessel and the “hot” submerged shield (corresponding to layer $X = 1$, $Z = 4$ in Fig. 4).

In Fig. 9 the calculated volumetric void fraction distribution is shown for the third ($Z = 3$) layer. Measured plant data, corresponding to the volumetric void fraction, α_g , in the central ($X = 5$) and “hot” ($X = 3$) corridors, are listed below together with the calculated values:

α_g	BAGIRA	NPP data
Central channel region	0.41	0.28
“Hot” channel region	0.59	0.58

It is seen that the calculated volumetric void fraction in the “hot” channel is in good agreement with the measurement. In the central channel the difference

between calculated and measured values of the void fraction is about 30%. However, the calculation was performed without specifically adjusting the free variable parameters (i.e. hydraulic resistance coefficients, turbulent mixing parameters, etc.), which could have been used to adjust the relative velocities of the coolant phases near the perforated plate to better match the experimental values. Considering this restriction, we can conclude that the calculation of the complex and nontrivial flow regime in the central channel reproduces the experimental data quite well.

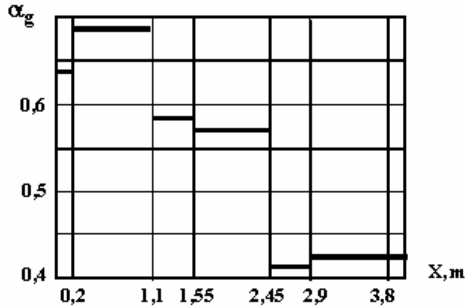


Fig. 9 Volumetric void fraction distribution (analysis)

The SG flow regime clearly shows multi-dimensional effects and the relatively good agreement between the calculated results and experimental data confirms the validity of the BAGIRA code for multi-dimensional analysis.

IV. FULL-SCOPE SIMULATOR FOR KALININ NPP

One of the new applications of BAGIRA code is its capability of simulating the primary reactor coolant circuits in real time enabling its use in plant simulators. Recently an analytic simulator model was developed for the Bilibino NPP using BAGIRA to model the thermal-hydraulic behavior of the reactor. However due to the specific design features of the Bilibino NPP reactor only the one-dimensional version of the code was applied. The full-scope simulator for the Kalinin NPP Unit No. 2 (VVER-1000) was developed with full two- and three-dimensional models for the reactor vessel and SG's, respectively.

The Kalinin simulator has been carefully tested using specific plant test procedures. As an example, Figs. 10 and 11 indicate the comparison of calculated and experimental results for a SG isolation test. In the test, all SG isolation valves are closed and consequently the steam flow-rate from all SG's is reduced to zero. This leads to an increase in the water level and pressure at the initial stage of the experiment ($t < 10$ s), since the feed water flow-rate remains constant. The increase in water level is clearly seen in the calculated curve in Fig. 11. The ex-

perimental data does not seem to indicate a similar increase in the measured water level, which is probably due to the rather long periods between successive measurements. As the secondary circuit pressure increases, the coolant temperature also increases near the heat-exchange tube bundle due to saturation conditions. As a result, the coolant temperature difference between the primary and secondary sides of the SG's is reduced leading to the reduction of heat transfer from the primary circuit and increase in pressure at $0 < t < 15$ s (Fig. 10). The reactor emergency protection and scram systems will act to reduce reactor power decreasing the primary circuit pressure.

When the secondary circuit pressure exceeds a certain predetermined level, emergency steam removal systems are activated, sharply increasing the steam flow-rate from the SG's, while the water level falls.

From Figs. 10 and 11 it is seen that BAGIRA code satisfactorily reproduces the qualitative phenomena observed in the SG's isolation valve closure test.

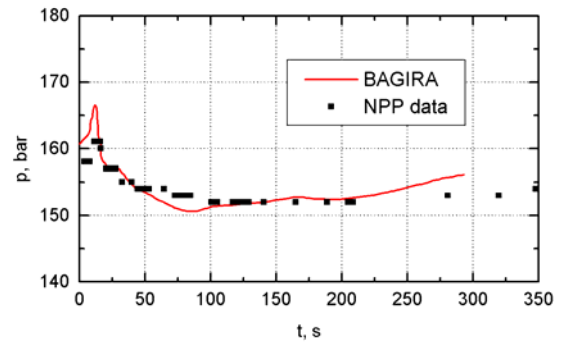


Fig. 10 Primary circuit pressure vs. time

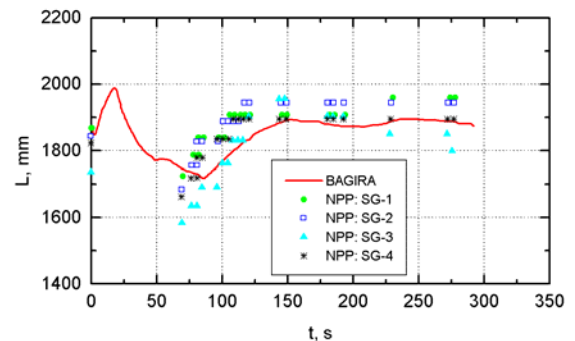


Fig. 11 Coolant levels in SG's vs. time

V. VERIFICATION OF BAGIRA CODE
 BASED ON EXPERIMENTS
 AT PSB-VVER INTEGRAL TEST FACILITY

Benchmark tests performed on integral test facilities play a significant role in the validating newly developed thermal-hydraulic best-estimate codes. Indeed, integral tests are normally characterized by investigating variety of physical phenomena, a wide range of measured parameters, and high measurement accuracy. Below we discuss the verification results of the BAGIRA code using data obtained in two recent experiments:

- (1) 1.3% leaks from primary circuit to secondary side,
- (2) Hot leg double-sided rupture, $2 \times 25\%$ break flow.

These tests were performed in 2001–2002 on the integral test facility PSB-VVER in Electrogorsk Research & Engineering Center (Electrogorsk, Moscow Region, Russia)³.

V.A. Description of PSB-VVER Test Facility

At present, the PSB-VVER facility is the most up-to-date Russian test unit capable of modeling the primary circuit of a typical VVER-1000 reactor. PSB-VVER is scaled as 1:300 in volume and power, and 1:1 in height to a VVER-1000 reactor.

Fig. 12 shows the isometric view of the PSB-VVER test facility. The facility consists of four circulation loops joined to the reactor vessel and core region. Each loop contains one RCP, SG, with “hot” and “cold” legs. In addition, it also includes a pressurizer that can be joined either to No. 2 or No. 4 loops. The emergency core coolant system (ECCS) consists of three sub-systems: a passive system with four hydro accumulators, and a coupled high and low-pressure injection systems.

The reactor model consists of a downcomer with the lower plenum, core region, core bypass and the upper plenum. The reactor core is simulated by 168 electrically heated fuel rods, which are separated by 15 spacer grids. The total heating power equals 1.5 MW (recently upgraded to 10 MW).

The PSB-VVER test facility is also equipped with special control systems allowing the modeling of specific accident responses (gas removal systems, pump shutdown systems, etc.).

A more detailed description of PSB-VVER and corresponding data can be found in References 3, 4.

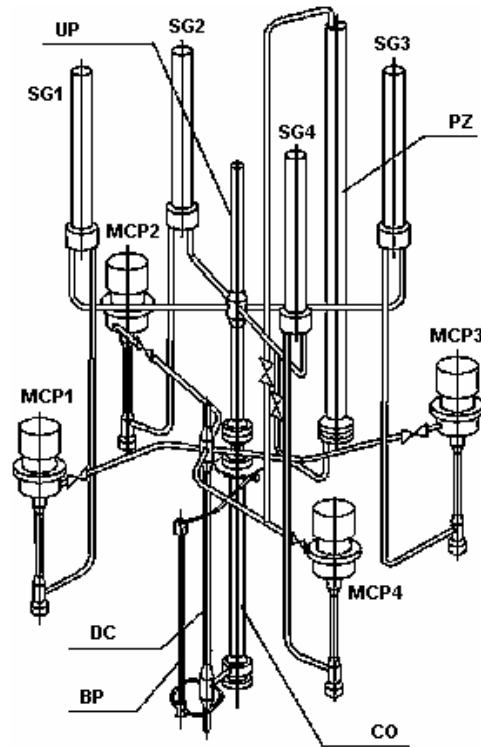


Fig. 12 General view of PSB-VVER integral test facility

- | | |
|-------------------|-------------------------|
| CO – core model | MCP – main coolant pump |
| BP – bypass | PZ – pressurizer |
| DC – downcomer | SG – steam generator |
| UP – upper plenum | |

V.B. Experiment PV-1.3-05, 1.3% leaks, from primary to secondary side

In experiment PV-1.3-05, the coolant, initially is in steady state with the following characteristics: upper plenum pressure 15.75 MPa, inlet/outlet coolant temperature at the core region 276/309 °C, fuel rod power 1497 kW, bypass power 30 kW, and secondary side pressure 6.3 MPa.

In the test a common vapor collector used for vapor removal connects all four SG’s to each other. The break is modeled by a 56 mm long pipe with the diameter of 5.8 mm with an isolation valve.

The experiment is initiated by opening the isolation valve in the break line at $t=0$ sec. Coolant starts flowing through the break opening from the primary to the secondary side leading to a rapid decrease of the primary circuit pressure as shown in Fig. 13a. Simultaneously, the water level in SG No. 4 increases (Fig. 13d). At $t=14$ sec into the accident (corresponding to 15th sec in the analysis) the pressure in the upper plenum falls to 14.7 MPa. This initiates a control sequence, first the

pressurizer heater is switched off, then the heating power in the fuel rods and bypass channel is reduced corresponding to a preset relationship, and the control sequence for RCP shutdown is initiated. On the secondary side, the feed water supply and steam extraction is shut down leading to an increase in SG pressure shown in Fig. 13c. Due to reduction in core power the coolant temperature at the core outlet is also reduced as seen in Fig. 13b.

At $t=54$ sec, the pressure in all SG's reaches 7.23 MPa corresponding to the activation of the steam dump system (quick-acting reduction valves) that reduces the secondary side pressure (Fig. 13c). Due to the coolant blowout through the steam dump lines, the rate of coolant level increase in SG No. 4 is also reduced. At the 99th sec of the experiment (102nd second in the calculation), the pressure in the primary circuit decreases to 7.8 MPa corresponding to the activation of the high-pressure ECCS. Cold water from the ECCS is pumped into the "hot" and "cold" legs of the No. 3 loop with flow-rates of 0.05 and 0.055 kg/s, respectively. Around the 120th second, the experiment pressure in the secondary circuit falls and the steam dump valves close (with slight differences in time between the different SGs). The pressure starts increasing again, Fig. 13c, due to the continuous coolant inflow from the primary circuit and the still considerable heat transfer between the primary and secondary side.

The continuous break flow eventually fills SG No. 4 to its top, Fig. 13d, and then proceeds to fill the other SG's through the common steam collector.

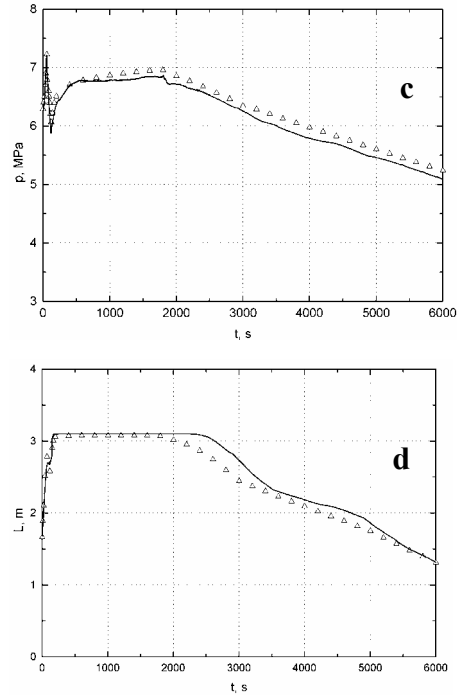
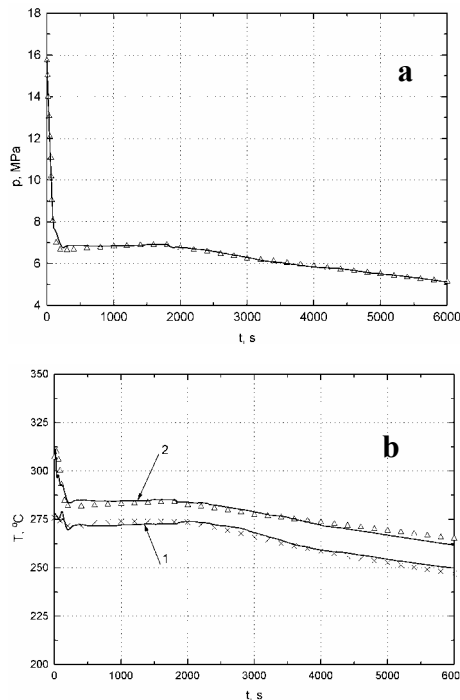


Fig. 13 PV-1.3-05 experiment, calculation vs. experimental data

- a – Primary circuit pressure;
- b – (1) inlet / (2) outlet coolant temperature;
- c – Secondary side pressure in SG No. 4 with break
- d – Coolant level in SG No. 4
- Solid line - calculations
- Triangles - experimental data



In spite of the continuing power decrease in the fuel rod assemblies, the coolant temperature (both in the calculation and experiment) increases slowly (Fig. 13b) caused by a decrease in coolant flow rate through the core region due to the shutdown of the RCPs. The increase in coolant temperature results in a corresponding pressure increase in the primary circuit (Fig. 13a). However, the pressure in the secondary side increases faster than in the primary resulting in a lower Δp between the two sides reducing the break flow. At about $t=1800$ sec the gas removal lines from the upper plenum and the SG collectors are opened by the operator, as part of the experimental procedure and the pressure, both in the primary and secondary circuits, begins to fall (Fig. 13a and c), the break flow reverses and the coolant now flows from the secondary to the primary side through the break in SG No. 4 leading to a decline in SG level as observed on Fig. 13d.

When the primary circuit pressure falls to 7.8 MPa, the accumulator isolation valves open and cold water starts entering the primary circuit. Water inflow from the

accumulators lasts until the water level is reduced to a preset level (one meter above the outlet) to prevent gas ingress in the primary circuit. However, when the accumulators are activated ($t=3812$ s) the upper plenum is already filled, and therefore no qualitative changes occur in the general physical condition of the overall system. After the system conditions stabilize, the experiment was stopped at $t = 6013$ s.

The table below lists the calculated and measured timing of events:

Event	Time, s	
	Experiment	Calculation
Break opening	0	0
Primary circuit pressure falls to 14.7 MPa. Pressurizer heater switched off, power reduction starts and RCP shut off	14	15
Pressure in SG's reaches 7.23 MPa. Steam dump system activated	54	54
Pressure in the primary circuit decreases to 7.8 MPa. HP ECCS activated	99	102
Steam dump valves close	119-123	120
Gas removal lines from the upper plenum and the SG collectors opening close. Flow reverse in the break line	1795-1805	1800
Accumulators activate	3750-3850	3812
Experiment is stopped	6013	6013

In general, we may conclude that the BAGIRA code correctly reproduced the main features of the physical processes taking place in a SG tube rupture experiment. The analysis is in good qualitative and quantitative agreement with the experimental data including predicting the behavior of important coolant parameters (such as the time dependent behavior of the primary and secondary side pressure), and was also able to take into account the effect of the operation of various auxiliary systems (accumulators, gas removal, valves, etc.).

V.C. Experiment GT-2x25-02 t, hot-leg double-sided rupture, 2 × 25% break flow

In experiment GT-2x25-02, the coolant, initially is in steady state with the following characteristics: upper plenum pressure 15.78 MPa, inlet/outlet coolant temperature at the core region 290/317 °C, fuel rod and

bypass power, respectively, 1520 and 16 kW, and secondary side pressure 7.84 MPa.

In this case the four SG's were joined to a common steam collector while the four accumulators were connected in pairs to the downcomer and upper plenum. The coolant blowdown and double-sided pipe rupture was modeled by two identical break lines opened simultaneously on the "hot" leg of the No. 3 loop.

At $t=0$ sec the isolation valves are opened simulating a double-ended pipe rupture. The initial coolant blowdown from the primary circuit leads to a sharp pressure drop as shown in Fig. 14a. At $t=.3$ sec the pressure drops to 13.73 MPa activating a sequence of events: first the ECCS initiated, then power is reduced in the core and bypass regions, shutdown sequence for the RCPs starts, signal for SG steam extraction lines closure is generated, and the pressurizer heaters are switched off. At about $t=.5$ sec, the primary circuit pressure reaches the saturation pressure (≈ 10.5 MPa) corresponding to the coolant temperature in the upper plenum and "hot" legs, and stabilizes for awhile.

By $t=1$ sec into the accident, the coolant is boiling in the SG heat-exchanger tubes, "hot" legs, upper plenum, and in the upper part of the core. At $t=20$ sec, the boiling front reaches the "cold" legs and the upper part of the downcomer. When the vapor phase appears in the primary circuit, the coolant temperature becomes equal to the saturation temperature and as the pressure drops its temperature reduces too. The fuel rod cladding temperature behaves similarly as seen on Fig. 14b.

At $t=15$ sec the coolant temperature in the SG tube bundle becomes less than the secondary side reversing the heat transfer process.

At $t=23$ sec the high pressure ECCS starts injecting water into "cold" leg No. 1 and vapor condensation on the cold water surfaces slightly increases the rate of pressure decrease in the primary circuit. At the same time, the ECCS water influx is unable to balance the break flow allowing the primary system water volume to decrease further.

At $t=38$ sec the passive accumulators activate and as cold water is injected into the primary water, vapor condenses decreasing the pressure even further. The accumulator has a significant effect on the primary circuit conditions, especially in the downcomer, as the cold water flows down to the lower plenum. The re-flooding of the core region and upper plenum is much more complicated as some parts of the injected water moves down into the lower plenum, while other parts cool the spacer grids and prevents the overheating of the fuel rods.

In the calculation the effect of the assembly geometry has been taken into account by an appropriately selected hydraulic resistance coefficient that allows the modeling of the water holdup in the core. The coefficient was adjusted to match the experimental data for the initial

steady-state pressure drop. Another factor that prevents the movement of water down to the lower plenum is the upward vapor flow generated in the core. The strong pressure oscillations seen between $t=50$ and 150 sec are due to two competing processes at the cladding surfaces with high temperature differences: intensive vapor condensation process followed by boiling, which is visible on Fig. 14c. By $t=140$ sec all the stored water from the accumulator is discharged and the tanks are isolated from the primary system.

As the pressure in the upper plenum falls below 2.16 MPa, the low-pressure ECCS is activated injecting cold water into the No. 3 “cold” and “hot” legs with the flow-rate 0.35 kg/s to each leg. The operation of the low-pressure injection continues to the end of the experiment.

The isolation of the accumulators leads to a relative stabilization (and even to a brief increase) of the primary circuit pressure. As the primary pressure decreases the Δp across the break openings becomes smaller reducing the break flow. At the same time the heat release continues in the core model and bypass increasing the coolant temperature and pressure.

After a short-term pressure increase in the primary system, the pressure starts to fall again due to the combined effect of coolant blowout through the break lines, vapor condensation on the surface of the injected ECCS cold water, and the decrease of the heating power in the fuel rod assemblies. At $t=340$ sec, the pressure reaches 0.4 MPa (pressure inside the containment), and the break lines are closed.

The low-pressure ECCS continues injecting water into the system and as the break lines are closed, primary circuit is re-flooded leading to a steady increase in primary system pressure. It is interesting to note the complex behavior of the re-flooding of the upper plenum middle part (Fig. 14c). The behavior of the pressure drop in the upper plenum may be explained by the ingress of some portion of the cold water from the low-pressure ECCS with the subsequent formation of a water “plug” supported by a rising vapor flux from the core region. As the “plug” water volume increases, it becomes unstable, and at about $t=800$ second the water discharges rapidly. This phenomenon does not reoccur, most likely due to the decrease in vapor generation. It is noteworthy that our analysis correctly reproduces this complex phenomenon.

As the water level gradually increases in the primary system, eventually it reaches the lower boundary of the SG tube bundles, heats up and starts boiling leading to a pressure and temperature increase in the primary circuit. This phenomenon results in a distinct step-like dependence of the pressure and temperature vs. time as can be seen in Fig. 14a&b near $t=810$ seconds for the

calculations. In the experiment, this phenomenon occurs a bit earlier, at about $t = 620$ second. We assume that this disagreement may be removed/minimized by applying a much finer spatial computational grid due to the large variations in the gradients of the important parameters (primarily coolant temperature). However, this slight discrepancy had only a small effect by shifting the time dependencies of some parameters and would not support a justification for modifying the spatial nodalization used in the model.

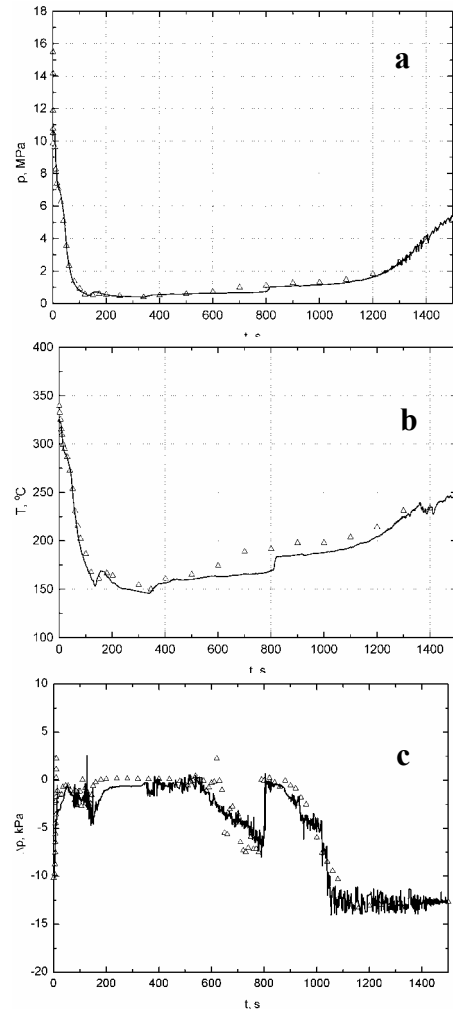


Fig. 14 a, b, c Comparison of calculation results with experimental data for GT-2x25-02 experiment:

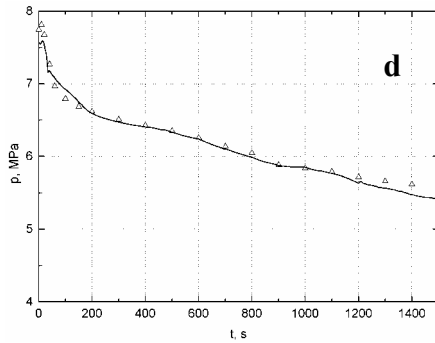


Fig. 14 d Comparison of calculation results with experimental data for GT-2x25-02 experiment:

- a – Primary circuit pressure
 - b – Fuel rod clad temperature
 - c – Pressure drop in upper plenum
 - d – Secondary circuit pressure
- Solid lines – calculation,
Triangles – experimental data.

Water flowing into the SG tubes enhances the heat exchange between the primary and secondary circuits leading to an increase in primary system pressure as seen in Figure 14d indicating a monotonic pressure decrease in the secondary side during the whole experiment. Since the SG's are joined by a common collector, the secondary side pressure is uniform for all SGs.

Note that both in the calculation and experiment the core region was at least partly submerged and no dry-out occurred preventing the occurrence of heat transfer crisis and insuring that the fuel rod cladding temperatures remained near the saturation line (Fig. 14b). The experiment was stopped at $t=1502$ second.

The table below lists the calculated and measured timing of events:

Event	Time, s	
	Experiment	Calculation
Break opening. Pressurizer heater is switched off. RCP shut off and vapor removal lines from SG's closed	0	0
Primary circuit pressure falls to 13.73 MPa. Power reduction starts.	0.4	0.3
HP ECCS activated	22	22
Pressure in primary circuit decreases to 5.88 MPa. Accumulators activated	35	38
LP ECCS activated	63	63
Water supply in hydro-accumulators is exhausted	130÷134	140
Primary circuit pressure falls to 0.4 MPa. Break line closure	335	340
HP ECCS switched off	473	473
Water level in primary circuit reaches lower boundary of SG tube bundle. Primary circuit pressure and coolant temperature start increasing	620	800
Experiment is stopped	1502	1502

The results obtained in our analysis indicates that the computer code BAGIRA, is able to correctly reproduce the whole set of various physical phenomena observed in this complex experiment. It is worth mentioning that the complex thermal-hydraulic processes in the experiment represented phenomena with quite different time scales. For instance, the primary circuit depressurization after the double-ended break took a fraction of a second, while the re-flooding of the primary circuit flood with ECCS water lasted more than one thousand seconds. In addition, one of the important characteristic features of the experiment was the strong, non-equilibrium coolant conditions that generally cause modeling difficulties.

IV. CONCLUSIONS

The validation results presented in this paper confirm that the computer code BAGIRA, is a powerful tool for numerical analysis of a wide range of phenomena important for the NPP safety. One of the main advantages of the code is multi-dimensional capability allowing modeling the flow patterns in complex geometries especially in nuclear reactor cores. As the various experiments indicate the use of complex multi-dimensional models are required for adequately analyze the thermal-hydraulic behavior of nuclear reactor cores under transient and accident conditions. It is also suggested that further multi-dimensional experiments would be extremely desirable to further validate complex computational models used to analyze nuclear reactor events.

REFERENCES

1. S. D. KALINICHENKO, P. Kohut, A. E. Kroshilin, V. E. Kroshilin, and A. V. Smirnov, "BAGIRA: A 3-D Thermal-hydraulic Code for Analysis of Complex Two-Phase Flow Phenomena", *Proc. of 2003 International Congress on Advances in Nuclear Power Plants (ICAPP'03)*, Paper 3352, Cordoba, Spain (2003).
2. "Investigation of hydrodynamic and thermal characteristics of SG-1000 separator at N-VNPP Unit 5", Final report No. 187-0217, OKB GIDROPRESS (1982).
3. V. N. BLINKOV, O.I. Melikhov, I.A. Lipatov *et al.* , "Investigation of VVER-1000 Steam Line Break Accident in the PSB-VVER Test Facility", *Proc. of 2003 International Congress on Advances in Nuclear Power Plants (ICAPP'03)*, Paper 3018, Cordoba, Spain (2003).
4. V. N. BLINKOV, O.I. Melikhov, G.I. Dremin *et al.*, "Evaluation of Adequacy of the VVER-1000 Natural Circulation Simulation at the PSB-VVER Test Facility" , *ibid.*, Paper 3019.

This work was supported in part by the U.S. Department of Energy under contract DE-AC02-98CH10886.

U.S. Department of Commerce
National Technical Information Service
5285 Port Royal Road
Springfield, VA 22131
(800) 553-6847
Facsimile: (703) 605-6900
Online ordering:

DISCLAIMER

This report was prepared as an account of work sponsored by an agency of the United States Government. Neither the United States Government nor any agency thereof, nor any of their employees, nor any of their contractors, subcontractors or their employees, makes any warranty, express or implied, or assumes any legal liability or responsibility for the accuracy, completeness, or any third party's use or the results of such use of any information, apparatus, product, or process disclosed, or represents that its use would not infringe privately owned rights. Reference herein to any specific commercial product, process, or service by trade name, trademark, manufacturer, or otherwise, does not necessarily constitute or imply its endorsement, recommendation, or favoring by the United States Government or any agency thereof or its contractors or subcontractors. The views and opinions of authors expressed herein do not necessarily state or reflect those of the United States Government or any agency thereof.

<http://www.ntis.gov/ordering.htm>

FOR UNCLASSIFIED, UNLIMITED STI PRODUCTS

Available electronically at-

OSTI:

<http://www.osti.gov/bridge>

Available for a processing fee to U.S. Department of Energy and its contractors, in paper from-

U.S. Department of Energy
Office of Scientific and Technical
Information
P.O. Box 62
Oak Ridge, TN 37831
(865) 576-8401
Facsimile: (865) 576-5728
E-mail: reports@adonis.osti.gov

National Technical Information Service (NTIS):

Available for sale to the public from-